Applied Catalysis B: Environmental 341 (2024) 123355

Contents lists available at ScienceDirect

Applied Catalysis B: Environmental

journal homepage: www.elsevier.com/locate/apcatb

Encapsulation of carbon-nanodots into metal-organic frameworks for boosting photocatalytic upcycling of polyvinyl chloride plastic

Jibo Qin [b], Yibo Dou [a,*], Jianchi Zhou [a], Dan Zhao [b], Tobias Orlander [b], Henrik Rasmus Andersen [b], Claus Hélix-Nielsen [b], Wenjing Zhang [b,*]

[a] State Key Laboratory of Chemical Resource Engineering, Beijing University of Chemical Technology, Beijing 100029, PR China
[b] Department of Environmental and Resource Engineering, Technical University of Denmark, Lyngby 2800 Kgs, Denmark

ARTICLE INFO

Keywords:
Polyvinyl chloride
Mild pyrolysis
CDs/Zr-MOF photocatalyst
Acetic acid

ABSTRACT

Although polyvinyl chloride (PVC) ranks as the third most mass-produced synthetic plastic, the chemical upcycling of non-biodegradable PVC waste remains a significant challenge. Herein, carbon nanodots combined with the metal-organic framework (CDs/Zr-MOF) are fabricated for photocatalytic upcycling of PVC. Specifically, the ultra-small-sized CDs (~2.0 nm) are encapsulated into Zr-MOF pores via a mild pyrolysis strategy. The maintained MOF structure facilitates charge/mass transfer and improves the surface-to-volume ratio of active sites of CDs. The CDs/Zr-MOF exhibits high activity for PVC conversion of ~76.5% towards acetic acid with a yield of ~14%. The mechanism investigation indicates the generated •OH radicals can efficiently trigger cleavage of C-Cl/C-C bonds of PVC. Moreover, the reduction of the energy barrier for the hydroxylation reaction as a rate-limiting step contributed to improved PVC conversion performance. This work offers a feasible method for fabricating nanoparticle-embedded MOF-based photocatalysts and provides new insights into the chemical upcycling of plastics.

1. Introduction

Since the 1950 s, synthetic petroleum-based plastics have become ubiquitous and indispensable in modern society [1–3]. However, it is estimated that 90% of plastic waste is not recycled in an environmentally friendly way, thereby imposing heavy burdens on ecosystems [4,5]. Alternately, chemical recycling of plastic is recognized as a promising way to tackle the challenge of "white pollution" [6,7], in which post-consumer plastic products can be converted into high-value-added chemicals or corresponding monomers [8]. Nevertheless, these developed strategies face the challenges of converting polyolefin plastics due to their all-carbon backbones are not thermodynamically amenable [9]. In particular, polyvinyl chloride (PVC) has the lowest recycling rate in the vast majority of countries, even though it is the third most widely produced plastic in the world. The main reason is that upcycling of PVC is incompatible with traditional chemical upcycling processes [10]. Until now, chemical upcycling of PVC plastic waste has been predominantly focused on thermal catalysis [11–14], which requires high energy inputs (high temperature and high pressure) [15,16]. Meanwhile, random scission of the carbon chain of polymers leads to poor selectivity in relation to converted products [17]. In addition, the thermocatalytic conversion of plastics always results in the generation of large amounts of solid waste and exhaust gases, which inevitably lead to energy waste and environmental pollution [18]. Currently, photocatalysis is regarded as an economical and green method for upcycling plastics because it can convert solar energy into chemical energy for the upcycling of plastics under mild conditions [19–21]. However, the plastics upcycling process is inhibited by low quantum efficiency, low catalytic activity and poor selectivity, based on limited types of reported efficient photocatalysts such as Pt/TiO_2 [22] and Nb_2O_5 [23]. Most importantly, the poor understanding of the underlying photocatalytic upcycling mechanism hinders the rational design of suitable photocatalysts [24]. Therefore, developing advanced photocatalysts for upcycling plastic waste into valuable hydrocarbon fuels under a mild environment, as well as clearly resolving complicated reaction mechanisms, is needed to overcome some of the current significant challenges.

Metal-organic frameworks (MOF) have been intensively investigated in the photocatalytic field while still facing the challenge of low charge separation rate [25–28]. Various metal oxides and porous carbon-based materials derived from MOF precursors following pyrolysis treatment

* Corresponding authors.
E-mail addresses: douyb@buct.edu.cn (Y. Dou), wenz@dtu.dk (W. Zhang).

https://doi.org/10.1016/j.apcatb.2023.123355
Received 14 June 2023; Received in revised form 7 September 2023; Accepted 29 September 2023
Available online 1 October 2023

are fabricated to tackle the above issues [29]. However, the high-temperature treatment of MOF typically results in the loss of active sites and a decrease in specific surface area [30]. In this regard, it is necessary to develop a new strategy that not only retains the framework structure of MOF for effective mass/charge diffusion but also ensures a high number of active sites in photocatalysis. For example, our prior research demonstrated that the ZnO/UiO66-NH_2 as a photocatalyst facilitates the catalytic conversion of polyester plastic. However, it exhibited slow reaction kinetics due to the inherent chemical inertness and high dissociation energy of C–C bonds in plastic [31]. Consequently, enhancing the activity of MOF-based photocatalysts for efficient upcycling of plastic waste continues to pose significant challenges. Recent studies have suggested that carbon nanodots (CDs), as a novel nanomaterial, possess excellent light absorption properties and rapid electron transfer capabilities [32]. To date, the strategy of loading CDs as localized electron acceptors on the surface of MOF photocatalysts to improve the catalytic activity has been widely employed [33,34]. Nevertheless, agglomerated CDs particles and unstable links between CDs and MOF are frequently observed, resulting in undesired experimental results. These issues could be effectively mitigated by embedding CDs into the pores of MOF.

Herein, we aim to fabricate CDs-embedded MOF for high-selective upcycling of PVC into acetic acid (Scheme 1). The structure of the MOF derivatives can be regulated and controlled by precisely adjusting the pyrolysis temperature. As an example, the glucose/UiO66 (G/Zr-MOF) is selected as a precursor, in which the glucose (G) is decorated into Zr-MOF pores via post-synthesis. Then, the embedded G can be in-situ converted into ultra-small-sized CDs (~2.0 nm) via mild pyrolysis. Since the Zr-MOF framework is stable at a mild pyrolysis temperature (240 °C), the in-situ-formed CDs are confined in the skeleton of Zr-MOF. The MOF skeleton of CDs/Zr-MOF not only controls the size and dispersion of CDs but also improves the efficiency of substrate diffusion in photocatalysis. Meanwhile, CDs as electron trap centers are capable of improving the carrier separation rate. As the pyrolysis temperature increases up to 470 °C, the framework of CDs/Zr-MOF is completely damaged and converted to C/ZrO_2. Interestingly, the direct pyrolysis of the Zr-MOF to C/ZrO_2 requires a higher temperature (above 520 °C). Then, the photocatalytic activity of the MOF derivatives obtained is evaluated using PVC as the target plastic. The relationship between the structural features of MOF derivatives and their photocatalytic activity is disclosed in detail. In addition, we elucidate the specific pathway for upcycling PVC by CDs/Zr-MOF, especially the cleavage of the C–Cl and C–C bond, which is systematically investigated. This work would provide new insights into the fabrication of MOF-derived photocatalysts and elaborate the mechanism of photocatalytic upcycling of PVC plastics.

2. Experimental section

2.1. Synthesis of Zr-MOF

The Zr-MOF is fabricated through a reported strategy with several modifications [35]. Specifically, $ZrCl_4$ (46.6 mg) and 1,4-benzene dicarboxylic acid (37.4 mg) are dissolved into N, N-Dimethylformamide solvent (200 mL) via 30 min ultrasonic treatment (solution A). Subsequently, trimethylamine (5 μL) and acetic acid (25 mL) are sequentially added to solution A and kept stirring for 1 h to obtain solution B. After that, the mixture solution is transferred into a Teflon-lined autoclave (45 mL) and maintained at 120 °C for 24 h. The resulting Zr-MOF is collected, washed five times with ethanol and then dried at 60 °C for 12 h.

2.2. Synthesis of G/Zr-MOF

The G/Zr-MOF is fabricated via a post-synthesis strategy. Specifically, Zr-MOF (0.3 g) is dissolved in different concentrations of G solution (20 mL) (1, 10, 30, 50 mM, EtOH: H_2O = 9:1) and stirred for 24 h. The obtained G/Zr-MOF is collected, washed five times with ethanol and then dried at 60 ℃ for 12 h.

2.3. Synthesis of CDs/Zr-MOF

The CDs/Zr-MOF is fabricated via mild pyrolysis. The G/Zr-MOF precursor is pyrolyzed to 240 °C at a rate of 5 °C min^{-1} and kept for 4 h under an N_2 stream to obtain CDs/Zr-MOF(X). The X represents the mass fraction of CDs, which is determined by the increased percentage of the C mass fraction in the CDs/Zr-MOF compared with pure Zr-MOF (Table S1).

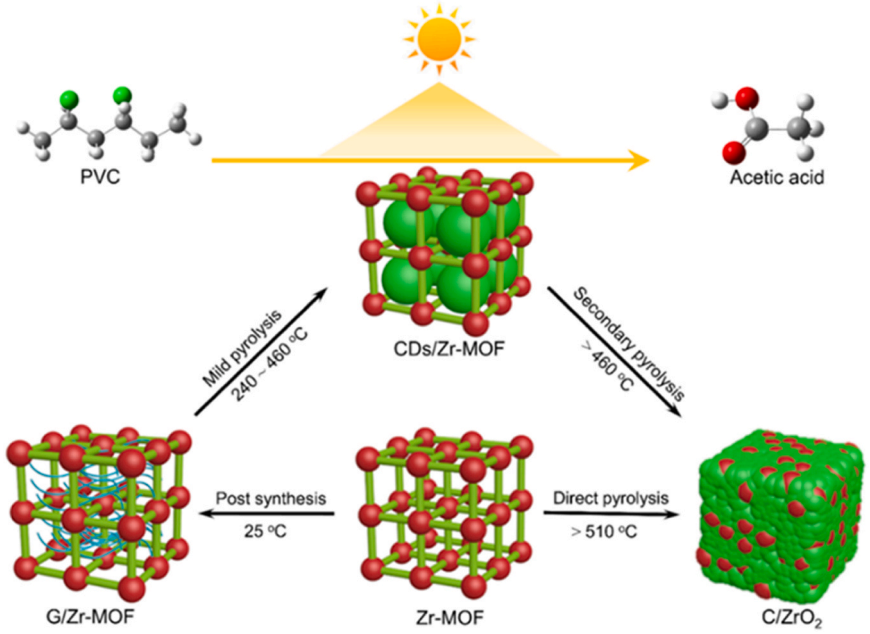

Scheme 1. The structural transformation of Zr-MOF into G/Zr-MOF, CDs/Zr-MOF and C/ZrO_2 by post-synthesis, direct pyrolysis, mild pyrolysis and subsequent secondary pyrolysis treatment, respectively. The resultant CDs/Zr-MOF displays high activity in the upcycling of PVC plastics towards acetic acid.

2.4. Synthesis of C/ZrO_2

The C/ZrO_2 is fabricated via secondary pyrolysis and direct pyrolysis. The CDs/Zr-MOF and Zr-MOF are pyrolyzed to 470 °C and 520 °C, respectively, and kept for 4 h under an N_2 stream to obtain C/ZrO_2.

2.5. Photocatalytic conversion of plastic

The upcycling PVC over the CDs/Zr-MOF is conducted in a self-made quartz reactor with a volume of 100 mL. In all, 1.0 g of photocatalyst and 0.2 g of PVC (Mn= 22000) are sequentially dispersed in a reactor filled with 50 mL of deionized water for photocatalysis. The temperature of the reaction system is controlled at room temperature using a temperature-controlled water bath. A 300 W Xe lamp (MC-PF 300 C, Beijing Merry Change Co., Ltd, working current: 21 A) is used as the light source. The distance from the light source to the reactor is 10 cm, and products of photocatalytic conversion of plastics are detected over a fixed time interval. Specifically, after the photocatalytic reaction, the suspension was sequentially centrifuged (1000 r min^{-1}) and filtered (0.22 μm) to remove plastic particles and photocatalyst. Subsequently, HPLC and IC were used to analyze the intermediate product and Cl^{-1}, respectively. During the analysis of the liquid samples, the small molecule organics in the liquid samples were directly analyzed by HPLC without further separation or purification. As for the photocatalyst recycling process, the suspension is filtered and centrifuged to obtain photocatalyst particles, which were dried at 65 °C for 12 h. Finally, the dried photocatalyst was used for the next cycle experiment.

3. Results and discussion

3.1. Fabrication and morphology characterization of photocatalysts

The CDs/Zr-MOF photocatalyst is fabricated via a MOF template-directed method (Fig. 1a). First, Zr-MOF is used as a substrate for the in-situ loading of G by the post-synthesis method to obtain G/Zr-MOF. The CDs/Zr-MOF is then fabricated by pyrolysis of G/Zr-MOF in an N_2 atmosphere through mild pyrolysis treatment. Scanning electron microscopy (SEM) shows that the particle size of the Zr-MOF (Fig. S1a) is

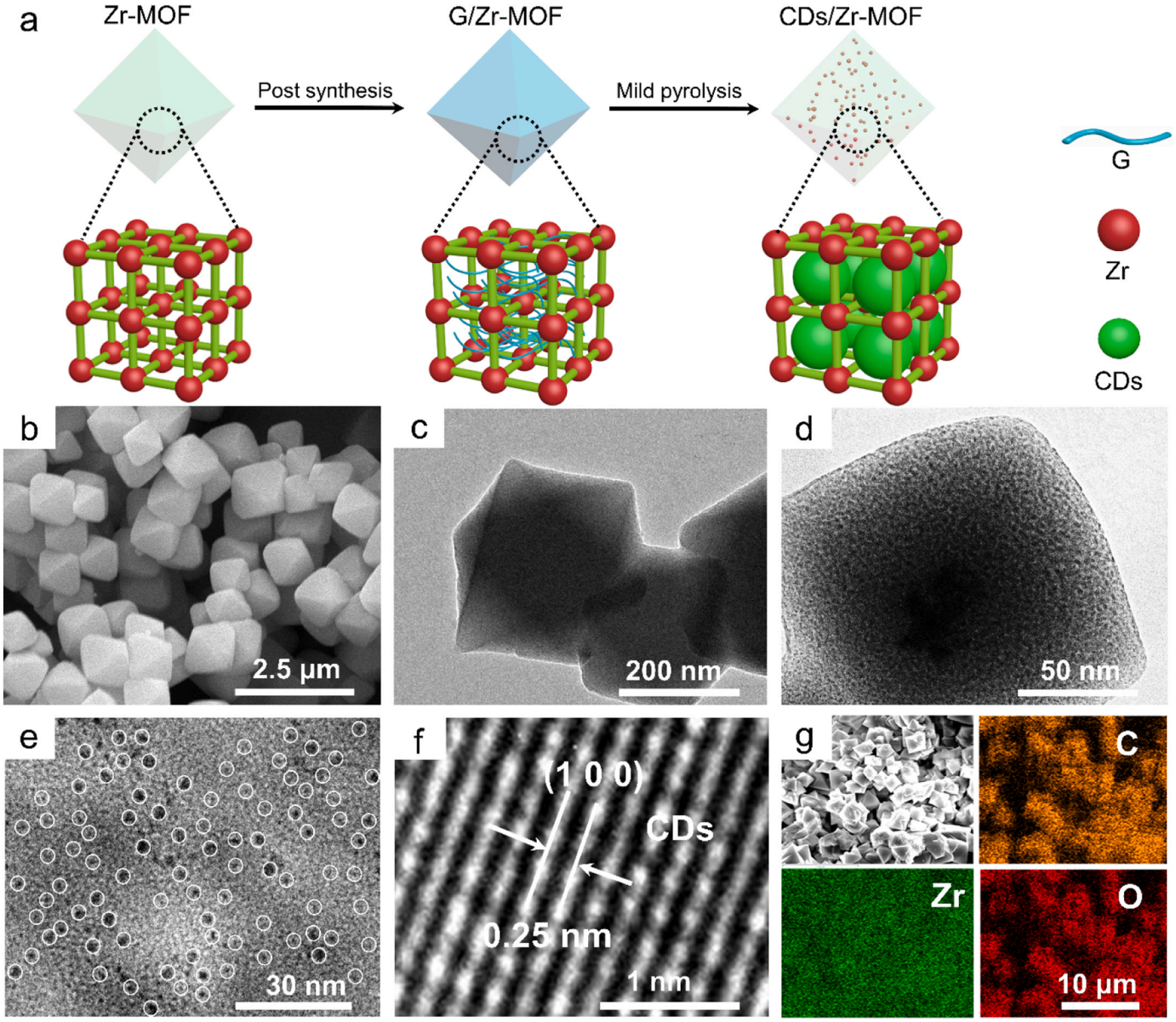

Fig. 1. (a) Schematic illustration for the fabrication of the CDs/Zr-MOF through the post-synthesis and mild pyrolysis treatment. (b) SEM image, (c, d) TEM images of CDs/Zr-MOF. (e) The distribution of the CDs inside of CDs/Zr-MOF. (f) HR-TEM image and (g) EDX mapping of CDs/Zr-MOF.

~1.0 μm with an octahedral shape, which is similar to the G/Zr-MOF (Fig. S2a) and CDs/Zr-MOF (Fig. 1b). The result indicates that the MOF structures of G/Zr-MOF and CDs/Zr-MOF are well preserved during post-synthesis and mild pyrolysis treatment. In addition, the structural changes and derivatization process of obtained MOF derivatives were recorded by transmission electron microscopy (TEM). No CD particles are observed inside the Zr-MOF (Fig. S1b-c). After pyrolyzing the G/Zr-MOF at 240 °C for 4 h, abundant CDs are observed, which are highly dispersed in the pores of the Zr-MOF with an average size of ~2.0 nm (Fig. 1c-e and Fig. S2b). The TEM images confirm that ultra-small-sized CDs can be formed at 240 °C. Simultaneously, the lattice fringe with an interplanar distance of ~0.25 nm is ascribed to the (1 0 0) crystal plane of CDs (Fig. 1f) [36], which suggests the formation of CDs inside CDs/Zr-MOF pores. Furthermore, energy-dispersive X-ray spectroscopy (EDX) mapping results demonstrate that Zr, C and O are homogeneously distributed on the entire CDs/Zr-MOF skeleton (Fig. 1g). To confirm the formation of CDs within the pores, the CDs/Zr-MOF was dispersed in a NaOH solution and subjected to ultrasonic water bath treatment to obtain the CDs by dissolving the MOFs framework of CDs/Zr-MOF. Then the CDs particles were obtained by filtration and extraction [37]. The size of CDs particle is ~2.0 nm (Fig. S2c), which is consistent with the TEM results of CDs inside CDs/Zr-MOF (Fig. 1e). When the temperature is raised to 470 °C, the morphology of the MOF becomes irregular (Fig. S2d), indicating that the MOF structure is about to decompose as a result of secondary pyrolysis. Interestingly, a higher temperature of 520 °C is required to completely damage the structure of the Zr-MOF following direct pyrolysis (Fig. S2e). In comparison to Zr-MOF, the thermal stability of the CDs/Zr-MOF

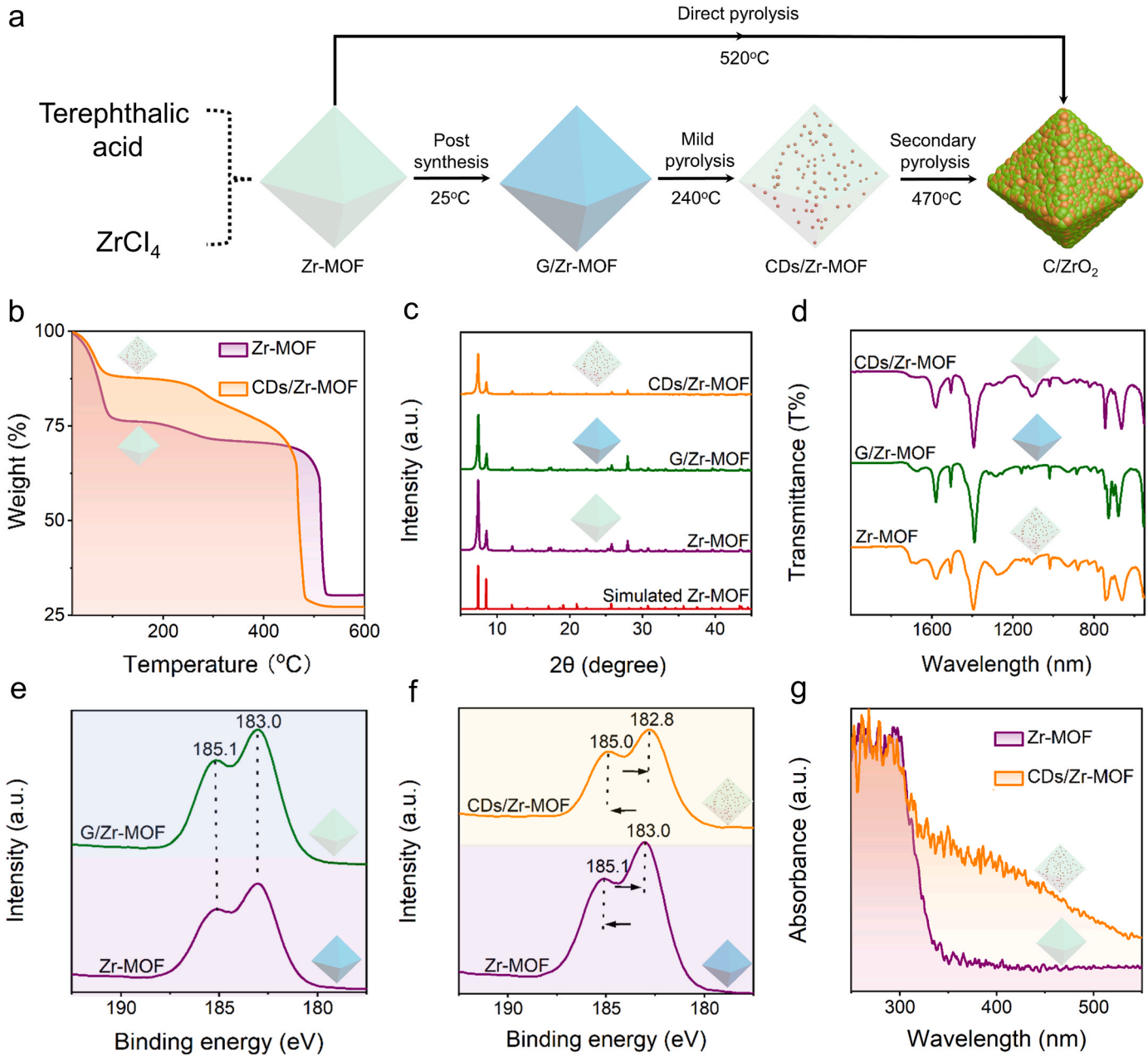

Fig. 2. (a) Schematic illustration of the fabrication of the Zr-MOF, G/Zr-MOF, CDs/Zr-MOF and C/ZrO_2 via different pyrolysis temperatures, respectively. (b) TGA curves of Zr-MOF and CDs/Zr-MOF, respectively. (c) PXRD patterns, (d) FTIR spectra of Zr-MOF, G/Zr-MOF and CDs/Zr-MOF, respectively. (e) Zr 3d XPS spectra of Zr-MOF and G/Zr-MOF, respectively. (f) Zr 3d XPS spectra of Zr-MOF and CDs/Zr-MOF, respectively. (g) UV–vis DRS spectra of Zr-MOF and CDs/Zr-MOF, respectively.

significantly decreased. This result suggests that the formation of CDs in CD/Zr-MOF pores leads to the lower thermal stability of the CDs/Zr-MOF, which will be discussed later.

3.2. The structural characterization of photocatalysts

To obtain the CDs/Zr-MOF by mild pyrolysis, ensuring a suitable pyrolysis temperature is significant. The thermogravimetric analysis (TGA) analysis shows that the G and CDs/Zr-MOF structures become unstable when the temperature exceeds 210 °C and 470 °C, respectively (Fig. 2a, b and Fig. S3). This result indicates that the CDs/Zr-MOF can be fabricated when the pyrolysis temperature of the G/Zr-MOF is controlled between 210 and 470 °C. Then, we select a pyrolysis temperature of 240 °C to synthesize the CDs/Zr-MOF. At this temperature, G can be carbonized into CDs embedded in CDs/Zr-MOF pores, while Zr nodes can retain the MOF skeleton. In this case, the MOF framework will be well-preserved for embedding CDs. In order to verify our assumption, the structures of transformed MOF derivatives via different pyrolysis method is investigated by powder X-ray diffraction (PXRD) (Fig. 2c and Fig. S4). The observed peaks of G/Zr-MOF and CDs/Zr-MOF match well with the pristine Zr-MOF, confirming that the original crystal structure of Zr-MOF is not affected during post-synthesis and subsequent mild pyrolysis treatment. Decreasing peak intensity of CDs/Zr-MOF indicates that in-situ-generated CDs reduce the crystallinity of MOF, and similar results can be observed in previous reports [32]. No diffraction peaks belonging to the CDs are observed due to the low content, which is also confirmed by Fourier-transform infrared spectroscopy (FTIR) (Fig. 2d). After pyrolysis of the Zr-MOF and CDs/Zr-MOF at 520 °C and 470 °C, respectively, their diffraction peaks of Zr-MOF disappear completely, along with the appearance of XRD peaks belonging to C/ZrO_2 (Fig. S4). This result indicates that the Zr-MOF and CDs/Zr-MOF are transformed into C/ZrO_2 during mild pyrolysis and secondary pyrolysis. Meanwhile, TGA analysis results indicate that the thermal stability of the CDs/Zr-MOF (470 °C) is lower than the pristine Zr-MOF (520 °C). The reason is the presence of CDs results in structural defects for the CDs/Zr MOF, in which the interaction between -COO^- and Zr^{4+} is weakened by embedded CDs [38]. The above TGA and PXRD analysis results, therefore, suggest that a suitable pyrolysis temperature is important for synthesizing porous CDs/Zr-MOF. Most importantly, mild pyrolysis can in-situ pyrolyze G into CDs, in which a well-maintained framework enables regulating the size and dispersion of embedded CDs.

Moreover, the chemical compositions and electronic interactions of the as-prepared photocatalysts were investigated. The X-ray photoelectron spectroscopy (XPS) shows the existence of C, Zr and O in the CDs/Zr-MOF (Fig. S5, Fig. 2e and Fig. 2f), which is consistent with the EDX analysis results (Fig. 1g). It should be noted that the introduction of G into the Zr-MOF pores does not affect the binding energy of the Zr-MOF (Fig. 2e). After mild pyrolysis, the binding energy of 3d 5/2 and Zr 3d 3/2 on the CDs/Zr-MOF shifts to the lower energy levels of 182.8 eV and 185.0 (Fig. 2f). This result indicates the occurrence of electron transfer from the Zr-MOF to CDs, owing to electronic coupling at the interface [39]. The observed variation in binding energy for Zr 3d indicates the well-integration between the Zr-MOF and CDs, which is beneficial for facilitating charge transfer and improving the structural stability of the CDs/Zr-MOF [40]. Furthermore, the optical properties of obtained photocatalysts were analyzed. The light absorption of the Zr-MOF shows an edge at ~345 nm. In comparison, the CDs/Zr-MOF and C/ZrO_2 display increasing absorption intensity in the absorption spectrum of 200–530 nm (Fig. 2g and Fig. S6). The results indicate that encapsulating CDs in the CDs/Zr-MOF is beneficial for improving their solar energy utilization due to the scatting effect generated by the porous structure and the up-conversion effect of embedded CDs [32].

3.3. Evaluation of photocatalytic performance for photocatalysts

Before the photocatalytic reaction, PVC is heated at 100 °C for 2 h to simulate the aging process of PVC waste in the natural environment. Fig. S7 shows the colour of the PVC changed from white to reddish brown after heating treatment, which indicates the PVC has been aged. It should be noted that heating treatment can affect the structural stability of PVC, leading to a decrease in mechanical strength [41,42]. The performance of synthesized CDs/Zr-MOF photocatalysts for upcycling PVC was then evaluated under full-spectrum illumination. The Zr-MOF exhibits weak activity with a PVC conversion of ~41.5% (Fig. 3a), mainly because of its poor light utilization capability and high electron-hole recombination rate. Notably, the activity of the CDs/Zr-MOF displays a volcano-shaped trend with increasing mass fraction (X) of CDs from 5% to 20% (Fig. 3a and Table S1). The best PVC conversion of ~76.5% is obtained when X = 10%, which can be attributed to that the maintained MOFs structure of CDs/Zr-MOF provides a channel for facile mass transfer. Meanwhile, CDs, as electron traps, can promote the electron separation of CDs/Zr-MOF. Further increasing X to 20%, the PVC conversion for CDs/Zr-MOF is decreased to ~53.0%, illustrating that excessive CDs inhibit the photocatalytic performance of CDs/Zr-MOF. The reason is probably that the overloaded CD may shield the incident light and act as a possible carrier recombination center. Fig. S8 shows the conversion rate of CDs/Zr-MOF for aged PVC was obviously improved compared with the PVC without heat treatment. It should be emphasized that pure CDs show no photocatalytic activity during PVC conversion. Next, the photocatalytic performance of optimal CDs/Zr-MOF (10%) photocatalyst is investigated in detail. As shown in Fig. 3b, the C/ZrO_2 exhibits poor photocatalytic activity with a PVC conversion rate of ~0.4 mg g_{cat}^{-1} h^{-1}. Therefore, the developed mild pyrolysis strategy can be used to synthesize nanoparticle-embedded photocatalysts with the comprehensive advantages of MOF and CDs nanoparticles. In addition, the PVC can not be converted without light or photocatalyst, indicating the upcycling of PVC by CDs/Zr-MOF should be driven by light. No obvious morphological changes are observed by comparing fresh (Fig. 2b)and used CDs/Zr-MOF (Fig. S9). Fig. S10 shows that the CDs/Zr-MOF has high catalytic stability, although there is a tiny variation in the PCV conversion rate after five successive cycles. These results thus indicate that the CDs/Zr-MOF displays high structural stability, accounting for stable PVC conversion activity. Moreover, the variation in Cl^{-1} concentration with reaction times was also analyzed. Fig. 3c and Fig. S11 show the Cl^{-1} concentration reaches 69.2 mg L^{-1} within 60 h. The obvious increase in Cl^{-1} concentration mainly occurred in the initial period of the catalytic reaction (0–20 h), while the conversion of PVC mainly occurred in the later stage (20–60 h). This result indicates that the conversion of PVC starts from a dechlorination reaction. Subsequently, the active radicals generated by the CDs/Zr-MOF participate in the cleavage of the C-C bond for the conversion of PVC. It is generally believed that C-Cl bond cleavage is caused either by the reduction of electrons or by the oxidation of active radicals. To explore the cleavage mechanism of the C-Cl bond in PVC, quenching experiments were carried out. Generally, benzoquinone (BQ), methanol (mL) and $KBrO_3$ can be used as scavengers of $\bullet O_2^-$, •OH and e^-, respectively. After adding BQ or $KBrO_3$ in this reaction system, the concentration of Cl^{-1} in the reaction system does not change significantly (Fig. S12). However, adding mL inhibits the positive effects of the CDs/Zr-MOF on Cl^{-1} release from PVC, suggesting that •OH plays an important role in the dechlorination reaction, which is consistent with previous reports [43]. In addition, the PVC conversion rate of the CDs/Zr-MOF is increased by ~10% in an O_2 atmosphere compared to air (Fig. S13). The result indicates that O_2 can promote the photocatalytic conversion of PVC. The detailed mechanism of how O_2 participates in PVC conversion will be discussed later.

Furthermore, FTIR spectroscopy was used to analyze functional group changes of PVC as a function of reaction time. The intensity of C–Cl peaks at 615 cm^{-1} decreases after the photocatalytic reaction, indicating that dehydrochlorination reactions occurred during the photocatalytic upcycling of PVC (Fig. 3d) [44], which is consistent with the results for upcycling PVC (Fig. 3c). Compared with fresh PVC, new

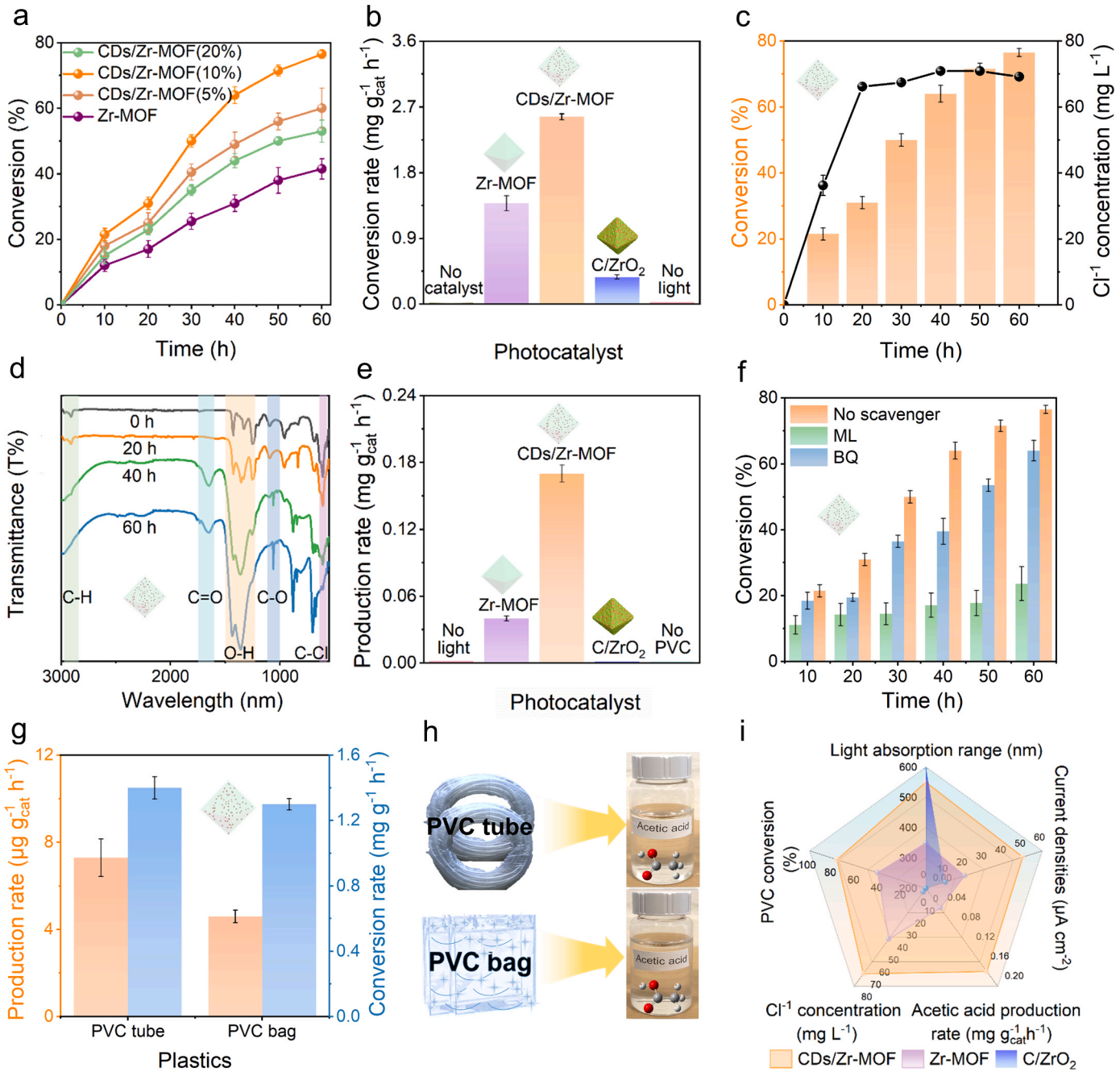

Fig. 3. (a) PVC conversion activity over Zr-MOF and CDs/Zr-MOF (X). (b) PVC conversion rates under C/ZrO_2, Zr-MOF and CDs/Zr-MOF, no light and no catalyst reaction systems, respectively. (c) The variation of Cl^{-1} concentration and PVC conversion over CDs/Zr-MOF as the function of reaction time. (d) The variation of FTIR spectra of PVC as the function of reaction time. (e) The acetic acid production rate under C/ZrO_2, Zr-MOF, CDs/Zr-MOF, no light and no PVC reaction systems. (f) PVC conversion activity over CDs/Zr-MOF in the presence of different scavengers. (g) The acetic acid production rate and PVC conversion rate over CDs/Zr-MOF in the PVC tube and PVC bag reaction system, respectively, and (h) images of collected acetic acid products. (i) The comparison of photocatalytic performance for C/ZrO_2, Zr-MOF and CDs/Zr-MOF, respectively.

peaks belonging to C-O bands (1015–1258 cm^{-1}) and C═O bands (1650 cm^{-1}) are observed in PVC with increasing reaction time [45], suggesting that PVC is gradually oxidized during photocatalysis. The peak at 1440–1395 cm^{-1} indicates the formation of the O-H band of carboxylic acid [46], caused by interactions between the PVC and active radicals. Moreover, the peaks at 2911 and 2848 cm^{-1} represent C-H groups and the asymmetric stretching of CH_2- in PVC [47]. The intensity of these peaks reduced after the photocatalytic reaction, indicating that a catalytic reaction occurs in the carbon chain of PVC. In addition, the products for the photocatalytic conversion of PVC were analyzed. The gel permeation chromatography (GPC) measurement shows the PVC is cleaved with a number-average molecular weight from 22000 to 528 within 60 h (Fig. S14), indicating the existence of soluble plastic fragments in the reaction system. Subsequently, HPLC technology was used to further analyze the intermediate products in this reaction system, which was followed by previously reported methods [48–51]. During the experiment, ethanol, acetic acid and formic acid were detected (Fig. S15), which is consistent with previous reports [48]. It should be emphasized that the yields or concentrations of ethanol, acetic acid and formic acid are much lower than those of acetic acid. Thus, the converted product is a complex organic system, which not only contains small molecular organic products (acetic acid, formic acid and ethanol,

etc.) but also contains soluble organic fragments. Considering the product contains complex polymer fragments, we did not provide a detailed discussion on product selectivity in this work. Up to now, there are few case of reports on product selectivity over photocatalytic PVC conversion [19,21,52–54]. How to regulate and optimize the product selectivity of plastic conversion should be the focus of our future research. Fig. 3e shows the acetic acid production rate for the CDs/Zr-MOF is ~0.17 mg g_{cat}^{-1} h^{-1}. In the comparison, the acetic acid yield of the CDs/Zr-MOF and Zr-MOF is ~14.0% and ~6.0%, respectively, indicating the CDs/Zr-MOF can effectively convert PVC plastic into high-value-added acetic acid (Fig. S16). Quenching experiments were carried out to verify the importance of active radicals in the photocatalytic process. Fig. 3f displays that after introducing mL and BQ, the PVC conversion rate of CDs/Zr-MOF decreased to 23.7% and 64.0%, respectively. This result demonstrates that $\bullet O_2^-$ and •OH are important active substances for PVC conversion. Considering the potential practical application, the CDs/Zr-MOF was further used to upcycle post-consumer PVC plastics. The ingredient of commercial PVC products is complex, and typically contain additional fillers, ester plasticizers, cross-linkers or antioxidants, etc [31,55,56]. Among them, the ester plasticizer undergoes a hydrolysis reaction with NaOH [57], which would affect the structural stability of commercial PVC products. Before the photocatalytic reaction, NaOH solution (1 M) is used to pretreat PVC tubes and bags for 24 h at 65 °C to reduce the mechanical strength and structural stability of PVC commercial plastics. As shown in Fig. S17, the conversion rate of commercial PVC products pretreated with NaOH is significantly improved. Fig. 3g shows the conversion rates of commercial PVC bags and PVC tubes are 1.3 and 1.4 mg g_{cat}^{-1} h^{-1}, respectively. Meanwhile, the CDs/Zr-MOF can convert these plastics into acetic acid with a production rate of ~4.6 and ~7.3 μg g_{cat}^{-1} h^{-1}, respectively (Fig. 3h), which confirms that the CDs/Zr-MOF has the potential for upcycling commercial plastic waste into acetic acid. In addition, it is difficult for CDs/Zr-MOF to convert polyethylene (PE) compared with PVC (Fig. S18). The reason is probably that PE only contains strong C–H (414 kJ mol^{-1}) and C–C (348 kJ mol^{-1}) bonds, which ensures the structural stability of the PE [31,58]. In the comparison, the bonding energy of the C-Cl (328 kJ mol^{-1}) bond of PVC is low, which is more easily cleaved during the photocatalytic process [43]. The dechlorination reaction can promote the cleavage of the PVC carbon chain as the dechlorination reaction reduces the structural stability of PVC [59]. Therefore, the conversion rate of CDs/Zr-MOF to PVC is higher than that of PE. In summary, compared with the Zr-MOF and C/ZrO_2, the CDs/Zr-MOF exhibits an improved activity in upcycling PVC (Fig. 3i). The reason is attributed to the maintained rich pores facilitates mass transfer and exposure of active catalytic sites. Meanwhile, encapsulated ultra-small-sized CDs improve the solar harvesting capacity (Fig. 2g). As a result, the synergistic effect between CDs and Zr-MOF suppresses the recombination of carriers (Fig. 4a), being beneficial for enhancing PVC conversion for CDs/Zr-MOF.

3.4. The investigation on photocatalytic properties of photocatalysts

To investigate the relationship between the structure and function, the carrier separation efficiency of prepared photocatalysts was investigated by photo-electrochemical characterization. The current ON-OFF densities (Fig. 3i and Fig. 4a) and the electrochemical impedance spectra

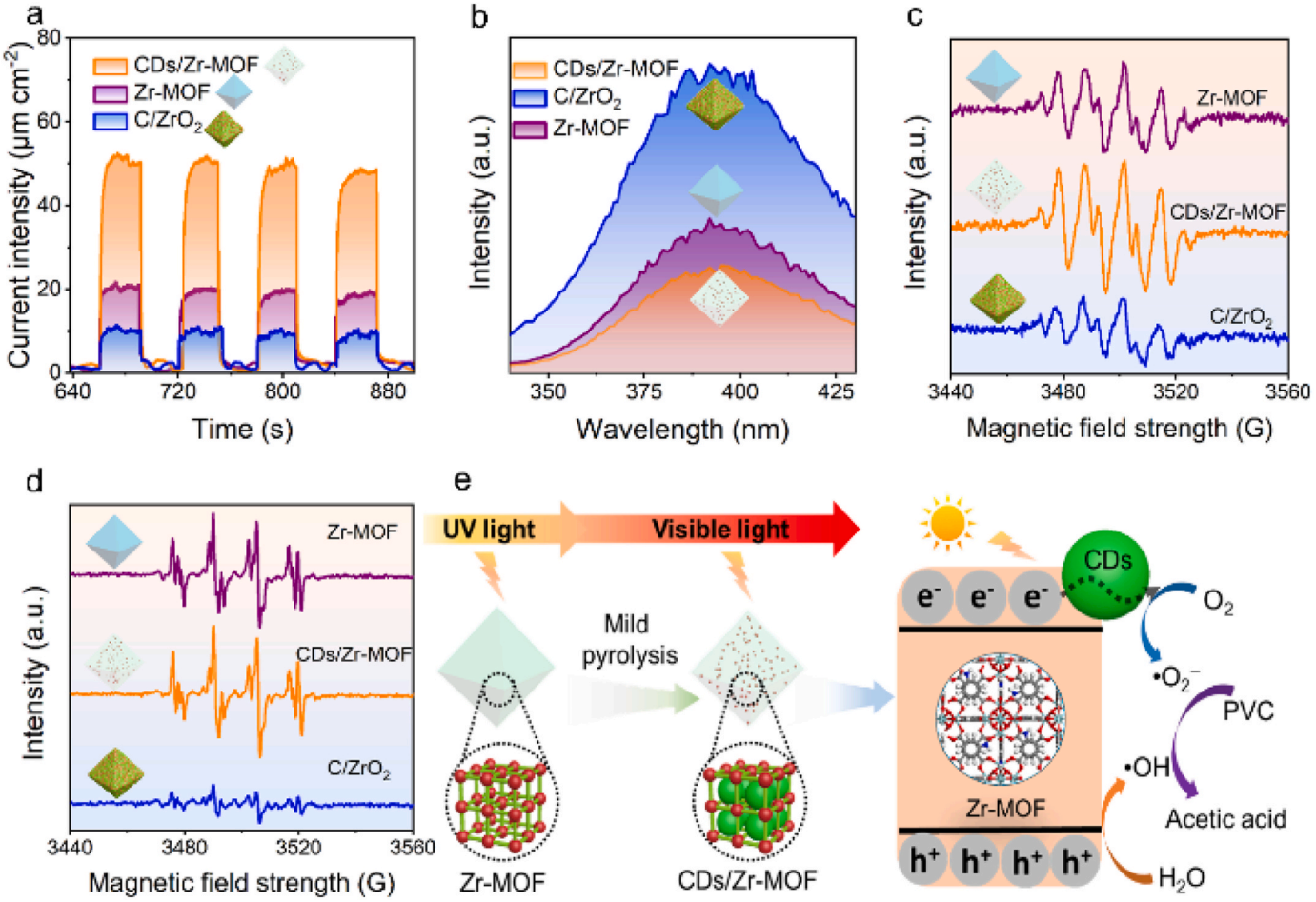

Fig. 4. (a) Transient photocurrent responses and (b) PL spectra of C/ZrO_2, Zr-MOF and CDs/Zr-MOF, respectively. ESR spectra of (c) DMPO-•O_2 and (d) DMPO-•OH for C/ZrO_2, Zr-MOF and CDs/Zr-MOF. (e) The mechanism of CDs/Zr-MOF photocatalytic conversion of PVC.

(EIS) results (Fig. S19) suggest that embedding CDs into Zr-MOF pores can promote the migration of charge carriers. Meanwhile, the CDs/Zr-MOF exhibits the lowest PL emission intensity (Fig. 4b) and the longest PL lifetime (Fig. S20). The results illustrate that CDs, as an electronic reservoir, can effectively prevent the recombination of electron-hole pairs [60]. Moreover, electron spin resonance (ESR) results suggest that the signal strength of •OH and $\bullet O_2^-$ can be increased after introducing CDs (Fig. 4c and Fig. 4d). Thus, the coupling of CDs and the Zr-MOF is beneficial for promoting surface electrons and holes to react with O_2 and H_2O to generate active radicals. In addition, the up-conversion effect of CDs on improving the generation rate of active radicals is shown in Fig. S21. Specifically, CDs can absorb long-wavelength sunlight (NIR-visible light) and emit short-wavelength light (UV–visible light) [61], which enables CDs/Zr-MOF to harvest visible light. As a result, the synergistic effect for CDs/Zr-MOF can enhance the generation and transfer of charge carriers for efficient

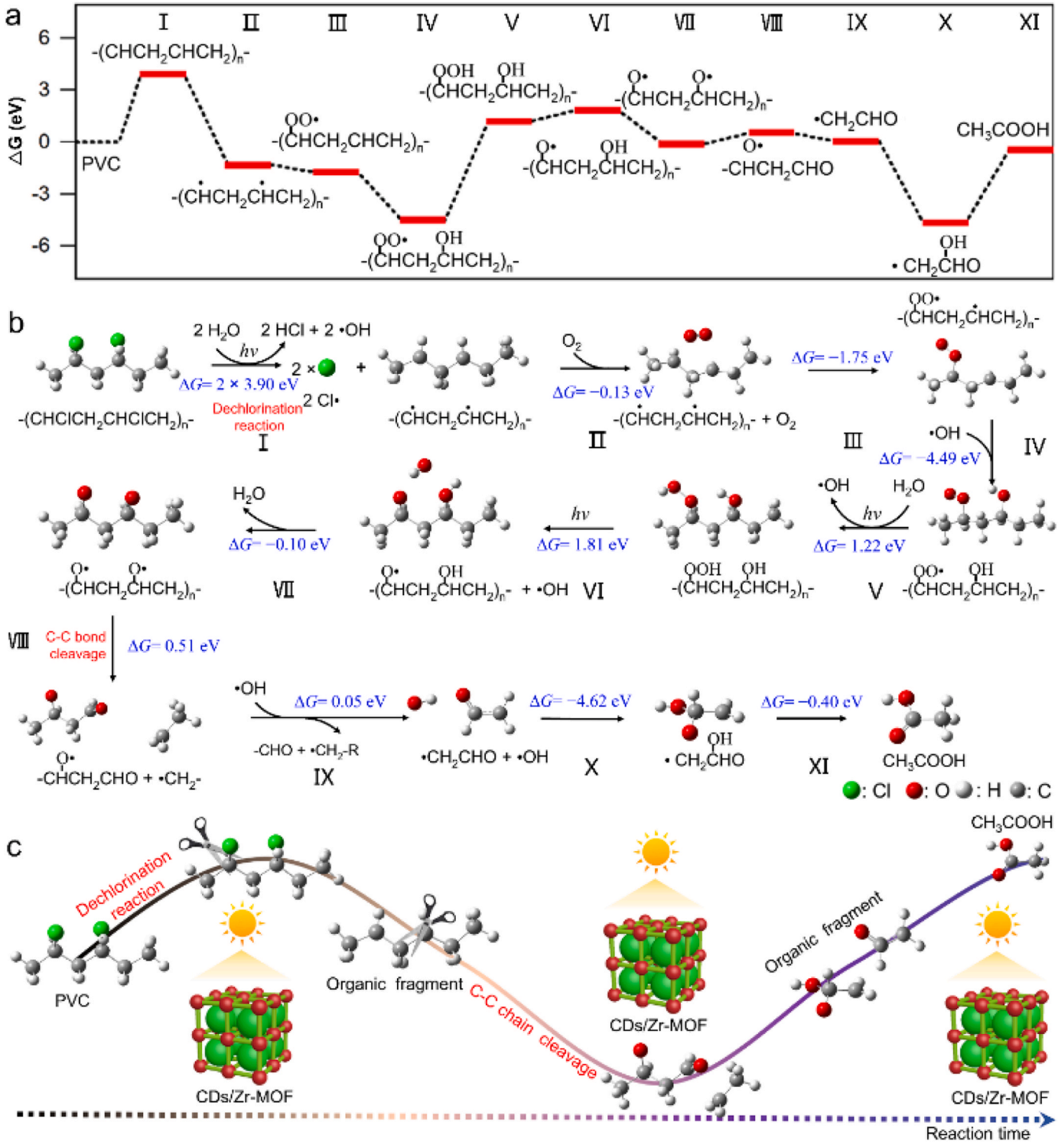

Fig. 5. (a) Gibbs free energy diagram and (b) elementary pathways for the photocatalytic conversion of PVC to acetic acid. (c) A simplified and visualized diagram of photocatalytic upcycling PVC over the CDs/Zr-MOF.

upcycling of PVC.

By combining the results of the UV-Vis (Fig. 2g), band gap energy (Fig. S22) and XPS (Fig. S23), the valence band (VB) and conduction band (CB) potential of CDs/Zr-MOF is calculated to be 3.0 and − 0.9 eV vs the normal hydrogen electrode (NHE), respectively, which ensures CDs/Zr-MOF can generate •OH and $\bullet O_2^-$ in this reaction system [62]. The band energy diagram for CDs/Zr-MOF with a possible electron-holes transfer mechanism is then proposed (Fig. 4e). Under light irradiation, the CDs/Zr-MOF can efficiently absorb visible light and UV light through the up-conversion effect of CDs to generate more electrons and holes than pure Zr-MOF (Fig. 4e), which enhances the photocatalytic activity of the CDs/Zr-MOF. According to previous reports, CDs act as electron mediators due to high electrical conductivity [61]. In this work, electrons are moved from the CB of the Zr-MOF to CDs. Then, the accumulated electrons in the CDs react with O_2 to generate $\bullet O_2^-$. Meanwhile, holes in the VB of Zr-MOF react with H_2O to generate •OH. In this case, the electrons and holes at the interface between CDs and Zr-MOF promote the charge transfer. Thus, charge carriers have a long lifetime to react with plastics. Under the synergistic effect of CDs and Zr-MOF, the electrons and holes are effectively separated, which affords an abundance of active radicals to convert PVC into acetic acid eventually.

3.5. The mechanism disclosure of PVC conversion

At present, due to the complexity and diversity of products and intermediates in chemical upcycling plastics, the identification of specific pathways for the photocatalytic conversion of plastics is facing a huge challenge [63–65]. According to previous reports, the theoretical calculation is one of the advanced strategies to simulate the plastics conversion pathways [23]. Based on the results obtained in this experiment, previous reports [48,66–70] and the theoretical calculations, a possible PVC conversion pathway is proposed in this work. Specifically, the CDs/Zr-MOF catalytic conversion of PVC towards acetic acid undergoes the following procedures (Fig. 5a, Fig. 5b and Fig. S24). Initially, the PVC polymer interacts with •OH radicals to generate the key intermediates, -(•$CHCH_2$•$CHCH_2$)$_n$- [66]. Subsequently, under the catalysis of the CDs/Zr-MOF, the -(•$CHCH_2$•$CHCH_2$)$_n$- can interact with O_2 with a low energy barrier (ΔG=−0.13 eV) and generate peroxide radicals [67–69], -(CH(OO•)-CH_2-•CH-CH_2)$_n$-, in which O_2 is an important species for stimulating initial activation of PVC. This is because the O_2 can be inserted into the α-ether C-H bonds to form hydroperoxides [70]. This result is consistent with the results of control experiments on investigation under the O_2 atmosphere (Fig. S13). After that, the -(CH(OO•)-CH_2-•CH-CH_2)$_n$- will undergo continuous hydroxylation and protonation under the photocatalysis of the CDs/Zr-MOF to generate -(CH(OOH)-CH_2-CH(OH)-CH_2)$_n$- irreversibly. The formation of -(CH(OOH)-CH_2-CH(OH)-CH_2)$_n$- is an exergonic process by 44.9 kcal mol^{-1} with respect to PVC [71]. Notably, the -(CH(OOH)-CH_2-CH(OH)-CH_2)$_n$- is a reactive intermediate for subsequent C–C bond cleavage, which is also reported by previous reports [72]. Specifically, under the catalysis of CDs/Zr-MOF, the -(CH(OOH)-CH_2-CH(OH)-CH_2)$_n$- is irreversibly converted into a key O-centered free radical -(CH(O•)-CH_2-CH(O•)-CH_2)$_n$-, which can undergo β-scission, leading to the C-C bond cleavage. Then, the -CH(O•)-CH_2-CHO, (•CH_2)-CHO and O═CHOH-CH_2• intermediates derived from C-C bond cleavage can be converted into acetic acid molecules undergo continuous hydroxylation and protonation reaction. In addition, the acetic acid desorption process is not only an endothermic process but also needs a large activation energy barrier [23], which makes it difficult for acetic acid to desorb from the surface of the CDs/Zr-MOF, thus affecting the generation rate of acetic acid. In summary, •OH radicals will preferentially cleave the C-Cl bonds, which initiates the photocatalytic conversion of PVC via introducing carbon-centred active radicals into the PVC carbon chain. Subsequent hydroxylation and protonation reactions result in the cleavage of the C-C bond and the final formation of acetic acid. It should be emphasized that the hydroxylation reaction is the rate-limiting step of acetic acid generation due to their high Gibbs free energy of − 4.49 and − 4.62 eV. Hence, a simplified pathway for upcycling PVC in the CDs/Zr-MOF photocatalytic reaction system is proposed (Fig. 5c). Initially, the C-Cl bond is preferentially cleaved by the active radicals generated by the CDs/Zr-MOF. The dechlorination reaction can accelerate the cleavage of the PVC carbon chain as the dechlorination reaction reduces the stability of PVC molecules [68]. Subsequently, under the synergistic effect of CDs and Zr-MOF, the long-chain polymer is oxidized into organic fragments containing oxygen-containing groups such as O-H, CH(O), CH(OOH) and O═C, which leads to the gradual cleavage of PVC carbon chains [48]. Ultimately, the organic fragments, such as -(CH(O•)-CH_2-CHO, (•CH_2)-CHO and O═CHOH-CH_2•), converted to high-value-added chemicals.

4. Conclusion

In this work, we designed and fabricated a CDs-embedded MOF composite for efficient upcycling of PVC. The structure of MOF derivatives can be regulated and controlled by adjusting pyrolysis temperature. Specifically, at a mild pyrolysis temperature, G can be converted into ultra-small-sized CDs encapsulated in Zr-MOF to obtain CDs/Zr-MOF. This mild pyrolysis strategy enables retaining abundant active sites and rich pores for efficient mass transfer. Meanwhile, the synergistic effect of Zr-MOF and CDs ensures that CDs/Zr-MOF exhibit a broad solar light absorption capability and a fast charge separation rate. As a result, the CDs/Zr-MOF shows high photocatalytic activity in converting PVC into acetic acid by effective cleavage of the C-Cl and C-C bonds of PVC. In addition, the CDs/Zr-MOF can effectively convert post-consumer PVC plastics, demonstrating the applicability and feasibility of our developed photocatalytic system in the field of chemical upcycling plastic wastes. This work thus provides new insights for the fabrication of MOF-based photocatalysts and converting waste plastics into high-value-added chemicals.

CRediT authorship contribution statement

Jibo Qin did photocatalytic experiments and wrote this manuscript. **Wenjing Zhang** and **Yibo Dou** gave valuable guidance in the photocatalytic experimental and directed and edited the manuscript. **Jianchi Zhou**, **Dan Zhao** and **Tobias Orlander** characterized photocatalysts. **Claus Hélix-Nielsen** and **Henrik Rasmus Andersen** directed and edited the manuscript.

Declaration of Competing Interest

The authors declare that they have no known competing financial interests or personal relationships that could have appeared to influence the work reported in this paper.

Data availability

Data will be made available on request.

Acknowledgements

This work was supported by the Novo Nordisk Foundation (NNF18OC0034918), the Innovation Fund Denmark Grand Solution (Grant No. 2079–00012B), the National Natural Science Foundation of China (22278029) and the Fundamental Research Funds for the Central Universities of China (buctrc202203). The author, Jibo Qin, would like to thank the funding support from the Chinese Scholarship Council for his stay at the Technical University of Denmark.

Appendix A. Supporting information

Supplementary data associated with this article can be found in the online version at doi:10.1016/j.apcatb.2023.123355.

References

[1] R. Shi, Z. Wang, Y. Zhao, G.I.N. Waterhouse, Z. Li, B. Zhang, Z. Sun, C. Xia, H. Wang, T. Zhang, Room-temperature electrochemical acetylene reduction to ethylene with high conversion and selectivity, Nat. Catal. 4 (2021) 565–574.
[2] K.L. Law, R. Narayan, Reducing environmental plastic pollution by designing polymer materials for managed end-of-life, Nat. Rev. Mater. 7 (2022) 104–116.
[3] K. Pabortsava, R.S. Lampitt, High concentrations of plastic hidden beneath the surface of the Atlantic Ocean, Nat. Commun. 11 (2020) 1–11.
[4] L. Yuan, L. Buzoglu Kurnaz, C. Tang, Alternative plastics, Nat. Sustain. 4 (2021) 837–838.
[5] J. Wang, L. Emmerich, J. Wu, P. Vana, K. Zhang, Hydroplastic polymers as eco-friendly hydrosetting plastics, Nat. Sustain. 4 (2021) 877–883.
[6] H. Lu, D.J. Diaz, N.J. Czarnecki, C. Zhu, W. Kim, R. Shroff, D.J. Acosta, B. R. Alexander, H.O. Cole, Y. Zhang, N.A. Lynd, A.D. Ellington, H.S. Alper, Machine learning-aided engineering of hydrolases for PET depolymerization, Nature 604 (2022) 662–667.
[7] M. Subramanian, Can nations rein in plastics pollution? Nature 611 (2022) 650–653.
[8] X. Zhao, B. Boruah, K.F. Chin, M. Đokić, J.M. Modak, H. Sen, Soo, Upcycling to sustainably reuse plastics, Adv. Mater. 34 (2022) 2100843.
[9] Z. Dong, W. Chen, K. Xu, Y. Liu, J. Wu, F. Zhang, Understanding the structure-activity relationships in catalytic conversion of polyolefin plastics by zeolite-based catalysts: A critical review, ACS Catal. 12 (2022) 14882–14901.
[10] M.K. Assefa, M.E. Fieser, Divergent silylium catalysis enables facile poly(vinyl chloride) upcycling to poly(ethylene-co-styrene) derivatives, J. Mater. Chem. A. (2023) 2128–2132.
[11] X. Liu, K. Tian, Z. Chen, W. Wei, B. Xu, B.J. Ni, Online TG-FTIR-MS analysis of the catalytic pyrolysis of polyethylene and polyvinyl chloride microplastics, J. Hazard. Mater. 441 (2023), 129881.
[12] M.J.B. de Souza, T.H.A. Silva, T.R.S. Ribeiro, A.O.S. da Silva, A.M.G. Pedrosa, Thermal and catalytic pyrolysis of polyvinyl chloride using micro/mesoporous ZSM-35/MCM-41 catalysts, J. Therm. Anal. Calor. 140 (2020) 167–175.
[13] W.H. Cheng, Y.C. Liang, Catalytic pyrolysis of polyvinylchloride in the presence of metal chloride, J. Appl. Polym. Sci. 77 (2000) 2464–2471.
[14] R. Yuan, Y. Shen, Catalytic pyrolysis of biomass-plastic wastes in the presence of MgO and $MgCO_3$ for hydrocarbon-rich oils production, Bioresour. Technol. 293 (2019), 122076.
[15] C. Park, H. Lee, N. Lee, B. Ahn, J. Lee, Upcycling of abandoned banner via thermocatalytic process over a MnFeCoNiCu high-entropy alloy catalyst, J. Hazard. Mater. 440 (2022), 129825.
[16] X. Jiao, K. Zheng, Z. Hu, S. Zhu, Y. Sun, Y. Xie, Conversion of waste plastics into value-added carbonaceous fuels under mild conditions, Adv. Mater. 33 (2021) 1–9.
[17] R. Cao, M.Q. Zhang, C. Hu, D. Xiao, M. Wang, D. Ma, Catalytic oxidation of polystyrene to aromatic oxygenates over a graphitic carbon nitride catalyst, Nat. Commun. 13 (2022) 4809.
[18] S.D. Anuar Sharuddin, F. Abnisa, W.M.A. Wan Daud, M.K. Aroua, A review on pyrolysis of plastic wastes, Energy Convers. Manag. 115 (2016) 308–326.
[19] Z. Ouyang, Y. Yang, C. Zhang, S. Zhu, L. Qin, W. Wang, D. He, Y. Zhou, H. Luo, F. Qin, Recent advances in photocatalytic degradation of plastics and plastic-derived chemicals, J. Mater. Chem. A 9 (2021) 13402–13441.
[20] F. Eisenreich, Photocatalysis as an effective tool for upcycling polymers into value-added molecules, Angew. Chem. - Int. Ed. 62 (2023), e202301303.
[21] S. Chu, B. Zhang, X. Zhao, H. Sen Soo, F. Wang, R. Xiao, H. Zhang, Photocatalytic conversion of plastic waste: from photodegradation to photosynthesis, Adv. Energy Mater. 12 (2022) 2200435.
[22] T. Kawai, T. Sakata, Photocatalytic hydrogen production from water by the decomposition of poly-vinylchloride, protein, algae, dead insects, and excrement, Chem. Lett. 10 (1981) 81–84.
[23] X. Jiao, K. Zheng, Q. Chen, X. Li, Y. Li, W. Shao, J. Xu, J. Zhu, Y. Pan, Y. Sun, Y. Xie, Photocatalytic conversion of waste plastics into C_2 fuels under simulated natural environment conditions, Angew. Chem. - Int. Ed. 132 (2020) 15627–15631.
[24] J. Qin, Y. Dou, F. Wu, Y. Yao, H.R. Andersen, C. Hélix-Nielsen, S.Y. Lim, W. Zhang, In-situ formation of Ag_2O in metal-organic framework for light-driven upcycling of microplastics coupled with hydrogen production, Appl. Catal. B Environ. 319 (2022), 121940.
[25] C. Zhang, C. Xie, Y. Gao, X. Tao, C. Ding, F. Fan, H.L. Jiang, Charge separation by creating band bending in metal–organic frameworks for improved photocatalytic hydrogen evolution, Angew. Chem. - Int. Ed. 61 (2022) 1–6.
[26] J. Liang, H. Yu, J. Shi, B. Li, L. Wu, M. Wang, Dislocated bilayer MOF enables high-selectivity photocatalytic reduction of CO_2 to CO, Adv. Mater. 35 (2023) 2209814.
[27] Z. Li, J. Zi, X. Luan, Y. Zhong, M. Qu, Y. Wang, Z. Lian, Localized surface plasmon resonance promotes metal–organic framework-based photocatalytic hydrogen evolution, Adv. Funct. Mater. 33 (2023) 2303069.
[28] H. Sepehrmansourie, H. Alamgholiloo, N. Noroozi Pesyan, M.A. Zolfigol, A MOF-on-MOF strategy to construct double Z-scheme heterojunction for high-performance photocatalytic degradation, Appl. Catal. B Environ. 321 (2023), 122082.
[29] J. Zhou, Y. Dou, A. Zhou, R.M. Guo, M.J. Zhao, J.R. Li, MOF template-directed fabrication of hierarchically structured electrocatalysts for efficient oxygen evolution reaction, Adv. Energy Mater. 7 (2017) 1602643.
[30] X. Wang, H. Xiao, A. Li, Z. Li, S. Liu, Q. Zhang, Y. Gong, L. Zheng, Y. Zhu, C. Chen, D. Wang, Q. Peng, L. Gu, X. Han, J. Li, Y. Li, Constructing $NiCo/Fe_3O_4$ Heteroparticles within MOF-74 for efficient oxygen evolution reactions, J. Am. Chem. Soc. 140 (2018) 15336–15341.
[31] J. Qin, Y. Dou, J. Zhou, V.M. Candelario, H.R. Andersen, C. Hélix-Nielsen, W. Zhang, Photocatalytic valorization of plastic waste over zinc oxide encapsulated in a metal–organic framework, Adv. Funct. Mater. 33 (2023) 2214839.
[32] Y. He, S. Luo, X. Hu, Y. Cheng, Y. Huang, S. Chen, M. Fu, Y. Jia, X. Liu, NH_2-MIL-125(Ti) encapsulated with in situ-formed carbon nanodots with up-conversion effect for improving photocatalytic NO removal and H_2 evolution, Chem. Eng. J. 420 (2021), 127643.
[33] W. Xu, J. Xu, Q. Zhang, Z. Yun, Q. Zuo, L. Wang, Study on visible light photocatalytic performance of MIL-100(Fe) modified by carbon nanodots, Environ. Sci. Pollut. Res. 29 (2022) 55069–55080.
[34] L. Shao, Z. Yu, X. Li, X. Li, H. Zeng, X. Feng, Carbon nanodots anchored onto the metal-organic framework NH_2-MIL-88B(Fe) as a novel visible light-driven photocatalyst: Photocatalytic performance and mechanism investigation, Appl. Surf. Sci. 505 (2020), 144616.
[35] Z. Man, Y. Meng, X. Lin, X. Dai, L. Wang, D. Liu, Assembling $UiO\text{-}66@TiO_2$ nanocomposites for efficient photocatalytic degradation of dimethyl sulfide, Chem. Eng. J. 431 (2022), 133952.
[36] W. Shi, F. Guo, M. Li, Y. Shi, M. Wu, Y. Tang, Enhanced visible-light-driven photocatalytic H_2 evolution on the novel nitrogen-doped carbon dots/$CuBi_2O_4$ microrods composite, J. Alloy. Compd. 775 (2019) 511–517.
[37] Z.G. Gu, D.J. Li, C. Zheng, Y. Kang, C. Wöll, J. Zhang, MOF-templated synthesis of ultrasmall photoluminescent carbon-nanodot arrays for optical applications, Angew. Chem. - Int. Ed. 56 (2017) 6853–6858.
[38] W. Xu, M. Dong, L. Di, X. Zhang, A facile method for preparing UiO66 encapsulated ru catalyst and its application in plasma-assisted CO_2 methanation, Nanomaterials 9 (2019) 10–13.
[39] Y. Dou, C. Grande, A. Kaiser, W. Zhang, Highly structured metal-organic framework nanofibers for methane storage, Sci. China Mater. 64 (2021) 1742–1750.
[40] C. Zhao, A. Zhou, Y. Dou, J. Zhou, J. Bai, J.R. Li, Dual MOFs template-directed fabrication of hollow-structured heterojunction photocatalysts for efficient CO_2 reduction, Chem. Eng. J. 416 (2021), 129155.
[41] M. Li, J. Jiang, J. Zhang, X. Yang, Y. Zhang, S. Li, J. Song, K. Huang, J. Xia, Preparation of a new liquid thermal stabilizer from rosin and fatty acid and study of the properties of the stabilized PVC, Polym. Degrad. Stab. 109 (2014) 129–136.
[42] N. Yarahmadi, I. Jakubowicz, T. Hjertberg, The effects of heat treatment and ageing on the mechanical properties of rigid PVC, Polym. Degrad. Stab. 82 (2003) 59–72.
[43] C. Wang, Z. Xian, X. Jin, S. Liang, Z. Chen, B. Pan, B. Wu, Y.S. Ok, C. Gu, Photo-aging of polyvinyl chloride microplastic in the presence of natural organic acids, Water Res 183 (2020), 116082.
[44] D. Ma, L. Liang, E. Hu, H. Chen, D. Wang, C. He, Q. Feng, Dechlorination of polyvinyl chloride by hydrothermal treatment with cupric ion, Process Saf. Environ. Prot. 146 (2021) 108–117.
[45] Y.Fei Chen, H. Yin, D.Lin He, H.Feng Gong, Z.Zhi Liu, Y.Qi Liu, X.Ming Zhang, W. Fen Pu, Low temperature oxidized coke of the ultra-heavy oil during in-situ combustion process: Structural characterization and evolution elucidation, Fuel 313 (2022), 122676.
[46] K. Rafińska, O. Wrona, A. Krakowska-Sieprawska, J. Walczak-Skierska, A. Kiełbasa, Z. Rafiński, P. Pomastowski, M. Kolankowski, B. Buszewski, Enzyme-assisted extraction of plant material – New functional aspects of the process on an example of Medicago sativa L, Ind. Crops Prod. 187 (2022), 115424.
[47] T.S. Renuga Devi, S. Gayathri, FTIR And FT-Raman spectral analysis of Paclitaxel drugs, Int. J. Pharm. Sci. Rev. Res. 2 (2010) 106–110.
[48] F. Miao, Y. Liu, M. Gao, X. Yu, P. Xiao, M. Wang, S. Wang, X. Wang, Degradation of polyvinyl chloride microplastics via an electro-Fenton-like system with a TiO_2/graphite cathode, J. Hazard. Mater. 399 (2020), 123023.
[49] B. Zhang, H. Zhang, Y. Pan, J. Shao, X. Wang, Y. Jiang, X. Xu, S. Chu, Photoelectrochemical conversion of plastic waste into high-value chemicals coupling hydrogen production, Chem. Eng. J. 462 (2023), 142247.
[50] C. Xing, G. Yu, J. Zhou, Q. Liu, T. Chen, H. Liu, X. Li, Solar energy-driven upcycling of plastic waste on direct Z-scheme heterostructure of V-substituted phosphomolybdic acid/g-C_3N_4 nanosheets, Appl. Catal. B Environ. 315 (2022), 121496.
[51] C.M. Pichler, S. Bhattacharjee, M. Rahaman, T. Uekert, E. Reisner, Conversion of polyethylene waste into gaseous hydrocarbons via integrated tandem chemical-photo/electrocatalytic processes, ACS Catal. 11 (2021) 9159–9167.
[52] H. Zhou, Y. Wang, Y. Ren, Z. Li, X. Kong, M. Shao, H. Duan, Plastic waste valorization by leveraging multidisciplinary catalytic technologies, ACS Catal. 12 (2022) 9307–9324.
[53] N. Li, H. Liu, Z. Cheng, B. Yan, G. Chen, S. Wang, Conversion of plastic waste into fuels: a critical review, J. Hazard. Mater. 424 (2022), 127460.
[54] F. Liu, X. Zhuang, Z. Du, Y. Dan, Y. Huang, L. Jiang, Enhanced photocatalytic performance by polarizing ferroelectric $KNbO_3$ for degradation of plastic wastes under mild conditions, Appl. Catal. B Environ. 318 (2022), 121897.
[55] T. Uekert, M.F. Kuehnel, D.W. Wakerley, E. Reisner, Plastic waste as a feedstock for solar-driven H_2 generation, Energy Environ. Sci. 11 (2018) 2853–2857.

[56] F. Zhu, Y. Yan, E. Doyle, C. Zhu, X. Jin, Z. Chen, C. Wang, H. He, D. Zhou, C. Gu, Microplastics altered soil microbiome and nitrogen cycling: the role of phthalate plasticizer, J. Hazard. Mater. 427 (2022), 127944.
[57] B. Cao, S. Wan, Y. Wang, H. Guo, M. Ou, Q. Zhong, Highly-efficient visible-light-driven photocatalytic H_2 evolution integrated with microplastic degradation over MXene/$Zn_xCd_{1-x}S$ photocatalyst, J. Colloid Interface Sci. 605 (2022) 311–319.
[58] F. Wu, C. Li, Y. Dou, J. Zhou, T. Jiang, Y. Yao, N.Y. Lee, S.Y. Lim, C. Hélix-Nielsen, W. Zhang, Solution plasma synthesis of Pt-decorated $Bi_{12}O_{17}Cl_2$ photocatalysts for efficient upcycling of plastics, Sci. Total Environ. 902 (2023), 165899.
[59] Y. Chen, S. Zhang, X. Han, X. Zhang, M. Yi, S. Yang, D. Yu, W. Liu, Catalytic Dechlorination and charring reaction of polyvinyl chloride by CuAl layered double hydroxide, Energy and Fuels 32 (2018) 2407–2413.
[60] M. Wang, J. Hua, Y. Yang, Fabrication of CDs/CdS-TiO2 ternary nano-composites for photocatalytic degradation of benzene and toluene under visible light irradiation, Spectrochim. Acta - Part A Mol. Biomol. Spectrosc 199 (2018) 102–109.
[61] X. Wei, Y. Wang, Y. Huang, C. Fan, Composite ZIF-8 with CQDs for boosting visible-light-driven photocatalytic removal of NO, J. Alloy. Compd. 802 (2019) 467–476.
[62] Q. Su, J. Li, B. Wang, Y. Li, L. Hou, Direct Z-scheme Bi_2MoO_6/UiO-66-NH_2 heterojunctions for enhanced photocatalytic degradation of ofloxacin and ciprofloxacin under visible light, Appl. Catal. B Environ. 318 (2022), 121820.
[63] K. Su, H. Liu, C. Zhang, F. Wang, Photocatalytic conversion of waste plastics to low carbon number organic products, Chin. J. Catal. 43 (2022) 589–594.
[64] F. Wu, Y. Dou, J. Zhou, J. Qin, T. Jiang, Y. Yao, C. Hélix-Nielsen, W. Zhang, High-entropy (FeCoNiCuZn)WO_4 photocatalysts-based fibrous membrane for efficient capturing and upcycling of plastic, Chem. Eng. J. 470 (2023), 144134.
[65] J. Chen, J. Wu, P.C. Sherrell, J. Chen, H. Wang, W.Xian Zhang, J. Yang, How to build a microplastics-free environment: strategies for microplastics degradation and plastics recycling, Adv. Sci. 9 (2022) 2103764.
[66] S. Cho, W. Choi, Solid-phase photocatalytic degradation of PVC-TiO_2 polymer composites, J. Photochem. Photobiol. A Chem. 143 (2001) 221–228.
[67] A.C. Albertsson, C. Barenstedt, S. Karlsson, Solid-phase extraction and gas chromatographic-mass spectrometric identification of degradation products from enhanced environmentally degradable polyethylene, J. Chromatogr. A. 690 (1995) 207–217.
[68] M. Scoponi, S. Cimmino, M. Kaci, Photo-stabilisation mechanism under natural weathering and accelerated photo-oxidative conditions of LDPE films for agricultural applications, Polymer 41 (2000) 7969–7980.
[69] P. Gijsman, G. Meijers, G. Vitarelli, Comparison of the UV-degradation chemistry of polypropylene, polyethylene, polyamide 6 and polybutylene terephthalate, Polym. Degrad. Stab. 65 (1999) 433–441.
[70] A. Sagadevan, K.C. Hwang, M. Der, Su, Singlet oxygen-mediated selective C-H bond hydroperoxidation of ethereal hydrocarbons, Nat. Commun. 8 (2017) 1–8.
[71] A. Rahimi, A. Azarpira, H. Kim, J. Ralph, S.S. Stahl, Chemoselective metal-free aerobic alcohol oxidation in lignin, J. Am. Chem. Soc. 135 (2013) 6415–6418.
[72] Z. Huang, M. Shanmugam, Z. Liu, A. Brookfield, E.L. Bennett, R. Guan, D.E. Vega Herrera, J.A. Lopez-Sanchez, A.G. Slater, E.J.L. McInnes, X. Qi, J. Xiao, Chemical recycling of polystyrene to valuable chemicals via selective acid-catalyzed aerobic oxidation under visible light, J. Am. Chem. Soc. 144 (2022) 6532–6542.